Neurobiology of Disease 162 (2022) 105585

Contents lists available at ScienceDirect

Neurobiology of Disease

journal homepage: www.elsevier.com/locate/ynbdi

ALS-linked cytoplasmic FUS assemblies are compositionally different from physiological stress granules and sequester hnRNPA3, a novel modifier of FUS toxicity

Haiyan An [a], Gioana Litscher [a], Naruaki Watanabe [b], Wenbin Wei [c], Tadafumi Hashimoto [b], Takeshi Iwatsubo [b], Vladimir L. Buchman [d,e], Tatyana A. Shelkovnikova [a,1,*]

[a] Medicines Discovery Institute, Cardiff University, Cardiff CF10 3AT, United Kingdom
[b] Department of Neuropathology, University of Tokyo, Tokyo, Japan
[c] Department of Biosciences, Durham University, Durham DH1 3LE, United Kingdom
[d] School of Biosciences, Cardiff University, Cardiff CF10 3AX, United Kingdom
[e] Belgorod State National Research University, Belgorod 308015, Russian Federation

ARTICLE INFO

Keywords:
FUS
ALS
Stress granule
RNP granule
FUS aggregate
hnRNPA3
SG core
Proteomics

ABSTRACT

Formation of cytoplasmic RNA-protein structures called stress granules (SGs) is a highly conserved cellular response to stress. Abnormal metabolism of SGs may contribute to the pathogenesis of (neuro)degenerative diseases such as amyotrophic lateral sclerosis (ALS). Many SG proteins are affected by mutations causative of these conditions, including fused in sarcoma (FUS). Mutant FUS variants have high affinity to SGs and also spontaneously form de novo cytoplasmic RNA granules. Mutant FUS-containing assemblies (mFAs), often called "pathological SGs", are proposed to play a role in ALS-FUS pathogenesis. However, structural differences between mFAs and physiological SGs remain largely unknown therefore it is unclear whether mFAs can functionally substitute for SGs and how they affect cellular stress responses. Here we used affinity purification to isolate mFAs and physiological SGs and compare their protein composition. We found that proteins within mFAs form significantly more physical interactions than those in SGs however mFAs fail to recruit many factors involved in signal transduction. Furthermore, we found that proteasome subunits and certain nucleocytoplasmic transport factors are depleted from mFAs, whereas translation elongation, mRNA surveillance and splicing factors as well as mitochondrial proteins are enriched in mFAs, as compared to SGs. Validation experiments for a mFA-specific protein, hnRNPA3, confirmed its RNA-dependent interaction with FUS and its sequestration into FUS inclusions in cultured cells and in a FUS transgenic mouse model. Silencing of the *Drosophila* hnRNPA3 ortholog was deleterious and potentiated human FUS toxicity in the retina of transgenic flies. In conclusion, we show that SG-like structures formed by mutant FUS are structurally distinct from SGs, prone to persistence, likely cannot functionally replace SGs, and affect a spectrum of cellular pathways in stressed cells. Results of our study support a pathogenic role for cytoplasmic FUS assemblies in ALS-FUS.

1. Introduction

Amyotrophic lateral sclerosis (ALS) is a rapidly progressive, incurable and inevitably fatal neurodegenerative disease affecting lower and upper motor neurons. Up to 90% of ALS cases are sporadic (sALS), and 10% are caused by mutations in known genes (familial ALS, fALS) (Hardiman et al., 2017). Despite recent genetic and molecular breakthroughs in dissecting ALS pathogenesis, underlying mechanisms shared by fALS and sALS are poorly understood, which represents a major obstacle in identifying universal therapeutic targets for this devastating disease (Taylor et al., 2016).

Stress granules (SGs) are cytoplasmic ribonucleoprotein (RNP) granules that form as a normal cellular response to stresses involving a shutdown of protein translation. SGs may serve to shield RNA from

* Corresponding author at: Sheffield Institute for Translational Neuroscience (SITraN), Department of Neuroscience, University of Sheffield, 385a Glossop road, Sheffield S10 2HQ, United Kingdom.
E-mail address: t.shelkovnikova@sheffield.ac.uk (T.A. Shelkovnikova).
[1] Present address: Sheffield Institute for Translational Neuroscience (SITraN), Department of Neuroscience, University of Sheffield, Sheffield, S10 2HQ, UK.

https://doi.org/10.1016/j.nbd.2021.105585
Received 2 September 2021; Received in revised form 2 December 2021; Accepted 11 December 2021
Available online 14 December 2021

degradation until protein translation can be safely resumed (Kedersha and Anderson, 2002) and to modulate stress signaling, including anti-apoptotic signaling, selective translation of molecular chaperones and adjustment of protein translation rates to prevent the accumulation of misfolded proteins (Kedersha et al., 2013).

Multiple SG proteins are affected by ALS-causative mutations (Li et al., 2013), including fused in sarcoma, or FUS (Kwiatkowski Jr et al., 2009; Vance et al., 2009). In the majority of ALS-FUS cases, the nuclear localisation signal (NLS) of FUS protein bears single amino acid substitutions or deletions, causing a defect in its nuclear import, uncontrollable deposition and inclusion formation in the cytoplasm – FUS proteinopathy (Lattante et al., 2013; Mackenzie et al., 2010). Unlike normal protein, mutant FUS isoforms mislocalised to the cytoplasm are readily recruited into stress-induced SGs (Bosco et al., 2010; Dormann et al., 2010). In addition, as we and others showed, overexpressed or endogenous mutant FUS spontaneously forms cytoplasmic micro-aggregates representing a novel type of RNP granule ('the FUS granule') that in stressed cells coalesce into larger assemblies comparable in size with mature SGs – 'FUS aggregates' (Japtok et al., 2015; Kino et al., 2015; Shelkovnikova et al., 2019; Shelkovnikova et al., 2014a; Takanashi and Yamaguchi, 2014). These collections of FUS granules are disruptive for physiological SGs because they compete with SGs for their core proteins such as G3BP1 and TIAR, as well as RNA species serving as a scaffold for SGs (Shelkovnikova et al., 2014a). The enrichment of mutant FUS in SGs may also alter their dynamics, affect the interactions between SG components and hence SG function (Aulas and Vande Velde, 2015; Baron et al., 2013). However, the detailed comparison of normal SGs and pathological FUS-containing SG-like structures has not been performed. It is still not clear whether the latter structures can substitute for the normal SG functions during stress, and the spectrum of cellular pathways they affect in stressed cells remains uncharacterized. Understanding the structural differences between normal SGs and their pathological, FUS-containing counterparts can provide us with important clues on mutant FUS-induced dysregulation of stress signaling.

In the current study, we interrogated the protein composition of biochemically purified mutant FUS cytoplasmic assemblies (mutant FUS containing SGs and clusters of FUS granules combined) – "mFAs", and compared their proteome to that of physiological SGs purified in parallel. This approach enabled the identification of a range of proteins enriched or depleted in mFAs, as compared to physiological SGs, and hence respective pathways impacted by mFA's presence in the cytoplasm of stressed cells. We also validated hnRNPA3, an RNA-binding protein specifically recruited to mFAs but not SGs and previously not implicated in ALS-FUS, in cellular, fly and mouse models of FUS proteinopathy. Our data suggest that formation of cytoplasmic FUS assemblies would have a profound effect on neurons under conditions of stress and support the role of these structures in ALS-FUS pathogenesis.

2. Results

2.1. Purification of stress granule and mutant FUS assembly cores and comparisons of their proteomes with published datasets

SGs were reported to consist of a collection of denser "cores" and a more diffuse "shell", with the relatively stable SG cores amenable to purification from mammalian cells (Jain et al., 2016). Mammalian SG cores measured based on G3BP1-GFP fluorescence are ~200 nm (233.1 ± 18.6 nm) in diameter (Jain et al., 2016). This is close to the size of spontaneously formed FUS granules formed by cytoplasmic FUS – ~150–200 nm (Shelkovnikova et al., 2019; Shelkovnikova et al., 2014a). Therefore, we reasoned that FUS granules can be enriched and purified using the protocol developed for SG cores. Only a proportion (~50%) of mutant FUS-expressing cells develop FUS granules or their clusters under basal conditions, whilst the remaining cells contain diffuse cytoplasmic FUS which becomes incorporated into SGs during stress (Shelkovnikova et al., 2014a). Therefore, in mutant FUS-expressing cells subjected to a SG-inducing stress, the SG core purification protocol will result in the isolation of both FUS granules (as constituents of FUS aggregates) and SG cores containing mutant FUS. This heterogeneous collection of mutant FUS-enriched structures is thereafter referred to as "mutant FUS assembly cores", or "mFA cores". As a driver for the formation of these structures we used FUS with an ALS-associated point mutation R522G with the confirmed ability to mislocalize to the cytoplasm and form FUS granules (Shelkovnikova et al., 2014a).

HEK293 cells were transfected to express either G3BP1-GFP or FUS (R522G)-GFP, and after 24 h, cells were treated with an oxidative stressor $NaAsO_2$ (sodium arsenite) for 1 h. SG and mFA formation was confirmed in these cultures by fluorescence microscopy (Fig. 1A). SG and mFA cores were purified by immunoprecipitation (IP) from cell lysates using GFP-Trap® beads, as schematically shown in Fig. 1B, and enrichment of GFP-tagged G3BP1 and FUS proteins in the final bead fractions was confirmed by western blot with an anti-GFP antibody (Fig. 1C). To ascertain successful purification of SG cores, we analyzed six transcripts previously reported as enriched in or depleted from SG cores in U2OS cells (Khong et al., 2017), using non-saturated PCR, in the cell lysate and SG_{core} fractions. This analysis fully reproduced the findings for U2OS SG cores where MACF1, BCL9L, CHD7 were enriched in SG cores and RPL39, UBL5 and GAPDH were depleted from these structures, as compared to the lysates (Fig. 1D).

Purified SG cores, mFA cores and the beads fraction from control (GFP only) samples were subjected to LC-MS/MS analysis. The "background' list of proteins obtained in 'GFP only' samples was subtracted from SG_{core} and mFA_{core} protein lists, yielding the final SG_{core} and mFA_{core} proteomes (Supplementary table S1). Comparison of our SG_{core} proteome with the SG proteomes from the original study (Jain et al., 2016) demonstrated significant overlaps – our dataset was found to include one-third (43/139) of the U2OS SG_{core} proteome ($p < 1.595e^{-32}$) and a quarter (103/411) of proteins from the "full SG proteome" ($p < 8.950e^{-68}$) (Fig. 1E). A larger size of our SG_{core} dataset and only partial overlap with the U2OS SG_{core} dataset may be explained by cell-specific differences and alterations introduced to the original protocol (see Materials and methods for details). Enrichr analysis on the overrepresented Biological Process Gene Ontology (GO) terms showed a substantial overlap between the HEK293 and U2OS SG_{core} datasets, where the top significant Biological Process GO terms in both datasets were related to regulation of translation (Supplementary Fig. S1). Encouragingly, one-third (45/144) of SG proteins from HEK293 cells identified through a different approach, APEX proximity labeling (Markmiller et al., 2018), were also included in our SG_{core} dataset ($p < 1.540e^{-32}$) (Fig. 1E). Our SG_{core} dataset also showed substantial enrichment in SG and P-body proteins from the HEK293 dataset obtained using another proximity-labeling methodology (Youn et al., 2018) (41/123 proteins, $p < 3.261e^{-34}$). It should be noted that individual overlaps between our SG_{core} dataset and published datasets (43, 45 and 41 proteins for Jain et al., Markmiller et al. and Youn et al., respectively) (Fig. 1E) do not correspond to the same list of proteins, as only 15 proteins were found to be in common for all three datasets.

We next aimed to establish the subset of proteins from the "basal" human FUS interactome that become sequestered into mFA cores. For that, we ran comparisons with the published datasets, namely, human FUS binding partners determined by tandem affinity purification with mass spectrometry using isotope labelling (SILAC) (Sun et al., 2015) and by FUS-GFP co-IP using anti-GFP nanobodies (Reber et al., 2021). mFA cores were found to include 45/323 and 93/360 proteins from these two datasets, respectively, which is significantly greater than expected by chance ($p < 2.740e^{-19}$ and $p < 3.426e^{-64}$, respectively) (Fig. 1F, Supplementary table S1). The three datasets had 31 proteins in common, and this shared set of proteins was highly enriched in RNA splicing and protein translation factors including well-established FUS interaction partners SMN1, RBM14, SYNCRIP, and DDX5 (Fig. 1F, Supplementary table S1). mFA cores also contained one-third (41/127) of FUS

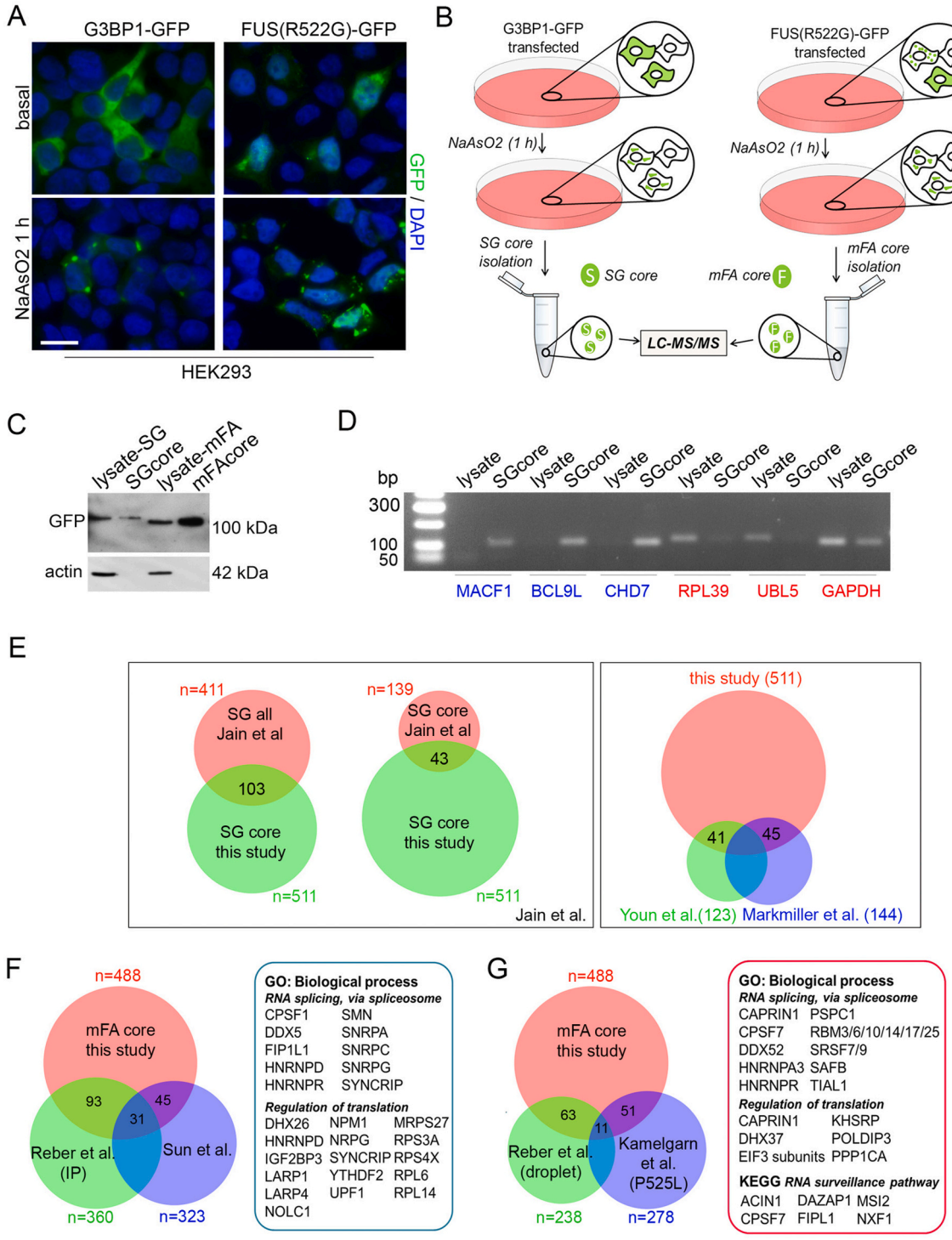

Fig. 1. Parallel purification and quality control of SG and mFA cores.
(A) Subcellular distribution of G3BP1-GFP and FUS(R522G)-GFP in HEK293 cells under basal conditions and under stress. Cells were transfected to express GFP-tagged proteins and 24 h post-transfection, treated with 0.5 mM $NaAsO_2$ for 1 h where indicated. Scale bar, 10 μm.
(B) Experimental pipeline for the isolation of SG and mFA cores for proteomic analysis.
(C) Efficiency of SG and mFA core pull-down analyzed by western blot with an anti-GFP antibody. 2% of the respective lysate was loaded in each case.
(D) Recruitment of transcripts known to be enriched in SG cores (blue) or depleted from SG cores (red) in U2OS cells (Khong et al., 2017) into HEK293 SG cores, as analyzed by non-saturated RT-PCR.
(E) Overlaps between the HEK293 SG_{core} proteomic dataset from the current study and published SG datasets.
(F) Overlaps between the mFA core proteome and published human FUS protein interactomes (Reber et al., 2021; Sun et al., 2015) and functional assignment of the proteins common for the three datasets ($n = 31$).
(G) Overlaps between the mFA core proteome and published interactomes of phase-separated/aggregated FUS species (Kamelgarn et al., 2018; Reber et al., 2021) and functional assignment of the mFA proteins appearing in at least one of these two published interactomes ($n = 92$).

interactors identified by co-IP in mouse cells (Blokhuis et al., 2016) (Supplementary table S1). We also purified total RNA from mFA cores and confirmed the enrichment of some known FUS mRNA targets in these structures (TIA1, MAPT, NVL) (Lagier-Tourenne et al., 2012), as compared to SG cores (Supplementary Fig. S2).

In a recent study, phase separated mutant FUS 'droplets' were purified and proteomically profiled using protein condensation from the lysate with subsequent fluorescent particle sorting (Reber et al., 2021). Aggregated mutant FUS fractions from mouse cells were also recently analyzed using a membrane filtration protocol (Kamelgarn et al., 2018). Comparison of the mFA_{core} proteome with these datasets also revealed significant overlaps, with 63/238 and 51/278 proteins included in the mFA_{core} dataset ($p < 5.580e^{-44}$ and $p < 1.820e^{-27}$, respectively) (Fig. 1G, Supplementary table S1). mFA core proteins appearing in these two datasets were significantly enriched in proteins involved in translation and RNA splicing, but also in the mRNA surveillance pathway (Fig. 1G).

Overall, these analyses confirmed a significant overrepresentation of known FUS binding partners from both total and insoluble/aggregated FUS interactomes within mFA cores.

2.2. Network-level comparisons of stress granule and mutant FUS assembly core proteomes

We next analyzed the SG_{core} and mFA_{core} proteomes using the STRING v11.5 database. For SG_{core} and mFA_{core} proteomes, 497/511 and 477/488 proteins, respectively, were mapped within the database. Visualization of protein-protein interactions for these mapped proteins using the STRING's graphical tool revealed that both types of RNP granules form tight networks of interactions (Fig. 2A). Among the top 25 enriched Biological Process GO term categories in the STRING database, five were shared by SG cores and mFA cores, namely *posttranscriptional regulation of gene expression*, *regulation of translation, mRNA metabolic process, amide biosynthetic process* and *peptide metabolic process*. SG_{core} and mFA_{core} proteomes were found to share 238 proteins, i.e. nearly half of all proteins in each dataset (Fig. 2B). The top Biological process GO term category for this common set of proteins, when analyzed in Enrichr, was *regulation of translation*, whereas the top Cellular Component GO term categories included *cytoplasmic ribonucleoprotein granules*, *cytoplasmic stress granules* and *P-bodies* (Fig. 2C).

We noticed that the "periphery" of the SG core network contained a large number of proteins with few or no interactions, which was not the case for mFA cores (Fig. 2A). Indeed, according to the STRING analysis statistics, proteins in mFA cores formed, on average, twice as many interactions as in SG cores, including "physical" interactions, i.e. when the proteins are known to exist in a complex (5.56 vs. 11.1 interactions per protein and 1381 vs. 2643 total interactions for SG_{core} and mFA_{core}, respectively) (Fig. 2D). The tighter network of physical interactions within mFA cores was clearly evident when only this type of interactions was visualized in STRING (Fig. 2E).

SGs are proposed to play an important role in signal transduction during stress (Kedersha et al., 2013). We counted the number of GO terms related to signaling in the list of overrepresented (false discovery rate, FDR < 0.05) Biological process GO terms in SG_{core} and mFA_{core} datasets. The SG_{core} dataset was found to contain 33 GO terms that mentioned signal transduction, as opposed to only 6 in the mFA_{core} dataset (Fig. 2D). For example, *estrogen receptor signaling pathway, NIK/NFkappaB signaling, Wnt pathway signaling, signal transduction in response to DNA damage, TNF-mediated signaling pathway, cytokine-mediated signaling pathway* appeared in the SG_{core} specific but not in the mFA^{core} specific list of overrepresented GO terms.

Thus despite a similar size of the SG_{core} and mFA_{core} proteomes and a multitude of shared proteins – known components of RNP granules involved in mRNA metabolism and gene expression regulation, these RNP granules appear drastically different in the density of protein-protein interactions and in their ability to concentrate signal transduction factors.

2.3. Cellular processes and pathways dysregulated by differential enrichment or depletion of specific proteins in mutant FUS assemblies during stress

We next focused on the SG_{core}-specific and mFA_{core}-specific sets of proteins. Using Enrichr and subsequently Revigo to remove redundant GO terms, we analyzed the list of 273 proteins found in SG cores but not in mFA cores. Non-redundant Biological Process GO terms enriched for this dataset included *regulation of ubiquitin protein ligase activity; protein sumoylation; cellular response to hypoxia; nuclear envelope disassembly;* and *regulation of gene silencing by RNA* (FDR < 0.01). In particular, we found that multiple proteasome subunit proteins (PSMA5, PSMA6, PSMA7, PSMB2, PSMB3, PSMB5, PSMC3, PSMD11, PSMD13) were recruited into SG cores, whereas only one proteasome subunit protein, PSMA4, was present in the mFA_{core} dataset (Fig. 3A). The second prominent category of proteins enriched in SG cores but not mFA cores were nuclear envelope proteins including NUP85, NUP107, NUP160, NUP214, and NUPL2 (Fig. 3A). In total, nine nuclear pore complex (NPC) proteins were found to be enriched in SG cores, and only five – in mFA cores. Consistently, KEGG pathway analysis also highlighted *Proteasome* and *RNA transport pathways* as enriched in proteins identified specifically in SG cores (Fig. 3B).

Capture and detainment of proteins by mFAs may result in their loss of function. Analysis of the mFA_{core}-specific proteome ($n = 250$) showed significant enrichment of Biological Process GO terms related to mitochondrial metabolism and more specifically, mitochondrial translation (Fig. 3A). Furthermore, mFA cores were significantly enriched in translation initiation factors including multiple members of the eIF-3 complex (EIF3A, EIF3C, EIF3G, EIF3H, EIF3I, EIF3K, EIF3L, EIF3M). Another group of proteins significantly enriched in mFA cores were the components of major (U2) and minor (U12) spliceosome subunits. In addition, we found that five Gemin proteins which interact with snRNPs to form the SMN complex are present in the mFA_{core} dataset, as opposed to only one in the SG_{core} dataset (Fig. 3A).

Finally, proteins within the *Spliceosome* and *mRNA surveillance pathway* KEGG pathways were significantly enriched in the mFA_{core} specific dataset (Fig. 3B). In particular, mFA cores were found to contain a number of multifunctional proteins with a critical role in RNA metabolism, such as NCBP1, NCBP2, HNRNPA3, SRSF9 (*Spliceosome*); and DAZAP1, CPSF1, CPS6, CPSF7 (*mRNA surveillance pathway*). We selected six mFA-specific proteins for validation by immunocytochemistry, namely NCBP1, HNRNPA3, EXOSC3, SAFB, CPSF6, and DAZAP1. SH-SY5Y cells were chosen over HEK293 cells since they are flatter cells with larger cytoplasm more suitable for imaging; it is also a cell line possessing some neuronal characteristics. All six proteins were found enriched in mFAs formed in $NaAsO_2$-treated SH-SY5Y cells (Supplementary Fig. S3). It should be noted that CPSF6 and DAZAP1 were previously detected in physiological SGs by immunocytochemistry (An et al., 2019b) but not in SG cores by proteomic analysis (Jain et al., 2016), suggesting that they are SG shell proteins. We further confirmed that these six proteins are recruited into compact FUS granule collections (FUS aggregates) formed in the absence of $NaAsO_2$ treatment (Fig. 3C).

Overall, this enrichment and validation analysis highlighted a number of factors and cellular pathways that can become dysregulated in cells in the presence of mFAs, most prominently mitochondrial protein homeostasis, translation and splicing. On the other hand, it highlighted the inability of mFAs to efficiently concentrate the proteasome and NPC proteins important for RNP granule disassembly and stress signaling.

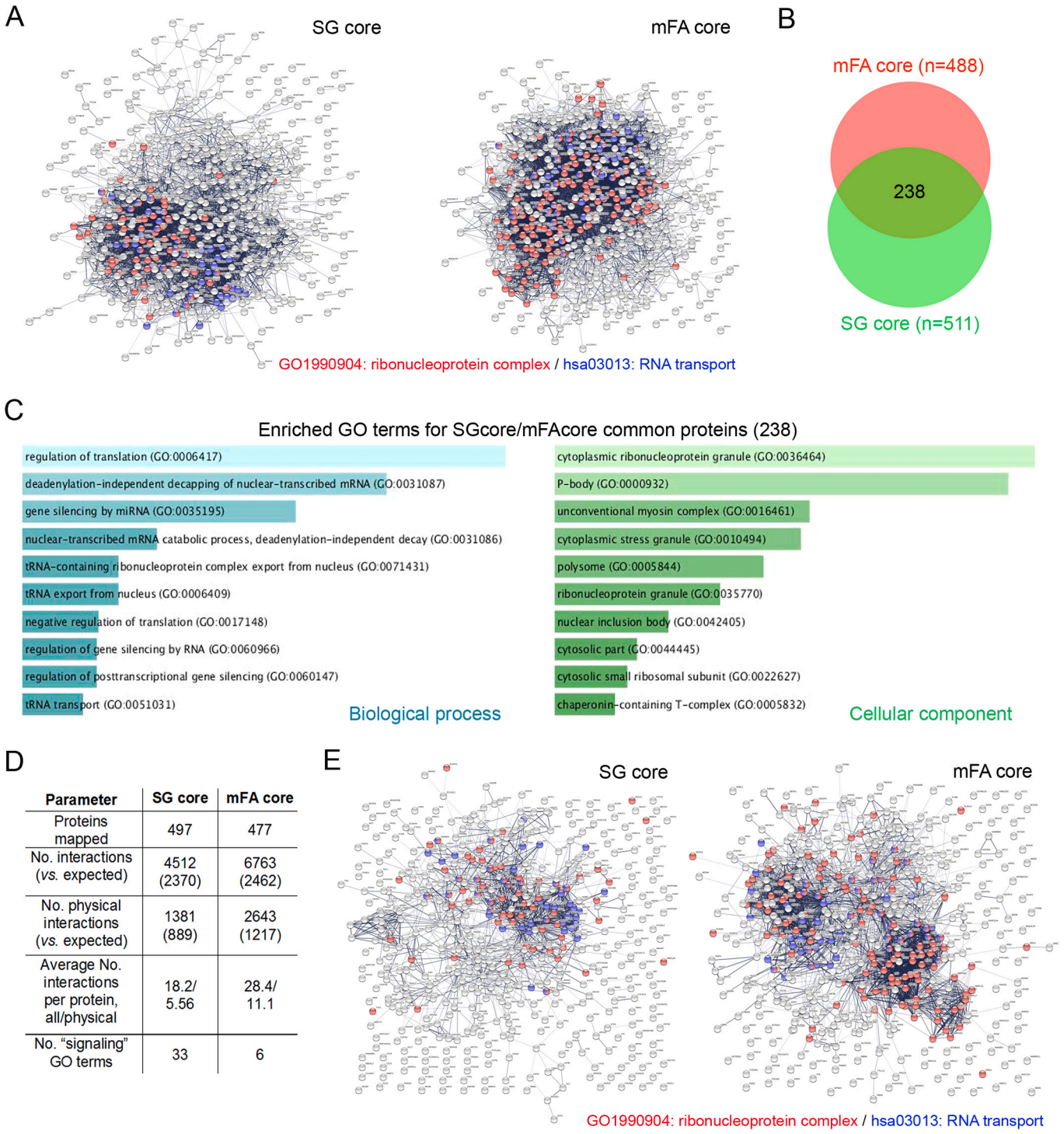

Parameter	SG core	mFA core
Proteins mapped	497	477
No. interactions (*vs.* expected)	4512 (2370)	6763 (2462)
No. physical interactions (*vs.* expected)	1381 (889)	2643 (1217)
Average No. interactions per protein, all/physical	18.2/ 5.56	28.4/ 11.1
No. "signaling" GO terms	33	6

Fig. 2. Network-level comparisons of the SG and mFA core proteomes.
(A) Protein interaction networks for SG and mFA cores visualized using the STRING graphical tool. 497/511 and 477/488 proteins were mapped for SG cores and mFA cores, respectively. Proteins from the overrepresented categories *Cellular component GO1990904: ribonucleoprotein complex* and *KEGG pathway hsa03013: RNA transport* are given in red and blue, respectively.
(B) Overlaps between the HEK293 SG_{core} and mFA_{core} proteomic datasets.
(C) Overrepresented Biological Process and Cellular component GO terms for proteins shared by SG and mFA cores, as determined using the Enrichr online tool.
(D) STRING statistics for SG_{core} and mFA_{core} datasets.
(E) Physical interactions networks for SG and mFA cores. Proteins from the overrepresented categories *Cellular component GO1990904: ribonucleoprotein complex* and *KEGG pathway hsa03013: RNA transport* are given in red and blue, respectively.

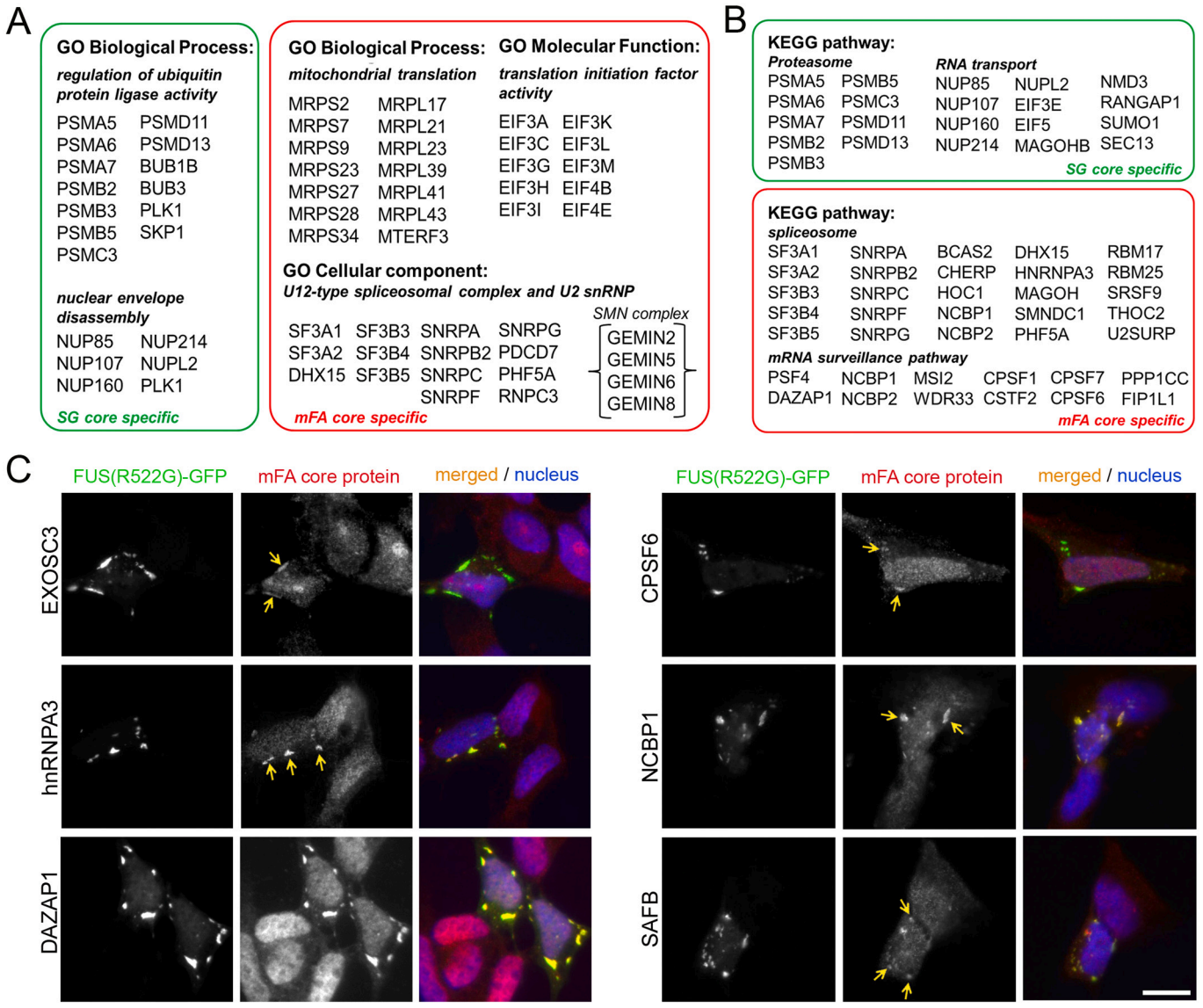

Fig. 3. Differential recruitment and depletion of cellular factors in SG cores and mFA cores.
(A) GO terms overrepresented in the SG_{core}-specific ($n = 273$) and mFA_{core}-specific ($n = 250$) proteomic datasets.
(B) KEGG pathways overrepresented in the SG_{core}-specific (n = 273) and mFA_{core}-specific (n = 250) proteomic datasets.
(C) Validation of mFA_{core}-recruited proteins. Sequestration of six proteins identified as mFA core components into FUS aggregates formed by transiently expressed FUS(R522G)-GFP was verified by immunocytochemistry in unstressed SH-SY5Y cells. Representative images are shown. Scale bar, 10 μm.

2.4. hnRNPA3 is sequestered into mutant FUS aggregates in cultured cells and a mouse model

We next focused on a mFA-specific protein that was previously implicated in ALS, hnRNPA3. hnRNPA3 has been identified as a component of C9ORF72 dipeptide repeat (DPR) inclusions and as a C9ORF72-repeat RNA interactor; it negatively regulates this RNA levels and DPR production, implicating its loss of function in ALS-C9 pathogenesis (Mori et al., 2013; Nihei et al., 2020). We first confirmed that hnRNPA3 is enriched in mFAs in $NaAsO_2$-treated cells and in FUS granules/FUS aggregates in unstressed cells, but not in $NaAsO_2$-induced G3BP1-GFP positive SGs (Fig. 4A). We noticed that hnRNPA3 often appears depleted from the nucleus of unstressed cells that contain large compact FUS aggregates. Quantification of fluorescence intensity in the nucleus indeed demonstrated a significant (38.2 ± 0.04%) decrease in nuclear hnRNPA3 in FUS aggregate-containing cells as compared to adjacent non-transfected cells (Fig. 4B). Co-expression of Flag-tagged hnRNPA3 and FUS(R522G)-GFP also confirmed co-localization of the two proteins (Fig. 4C).

To establish the functional domains of FUS responsible for its interaction with hnRNPA3 and its recruitment into FUS-enriched assemblies, we transiently expressed FUS deletion mutants localized to the cytoplasm (Fig. 4D), followed by anti-hnRNPA3 staining. This analysis showed that RRM and RGG domains of FUS are required for efficient recruitment of hnRNPA3 into FUS aggregates (Fig. 4D) and hence suggested that FUS-hnRNPA3 interaction is RNA-dependent. To address this directly, we performed IP of mutant FUS from samples treated or not treated with RNase A and examined the presence of endogenous hnRNPA3 in IP samples by western blot; WT FUS was included in this experiment to test whether a mutation increases FUS affinity to hnRNPA3 (Supplementary Fig. S4). WT and mutant (R522G) FUS precipitated hnRNPA3 with equal efficiency, and RNase A treatment completely abolished hnRNPA3 interaction both with normal and mutant FUS (Fig. 4E), corroborating the results of the experiment with FUS deletion mutants.

Although hnRNPA3 is enriched in mFAs in stressed cells and FUS

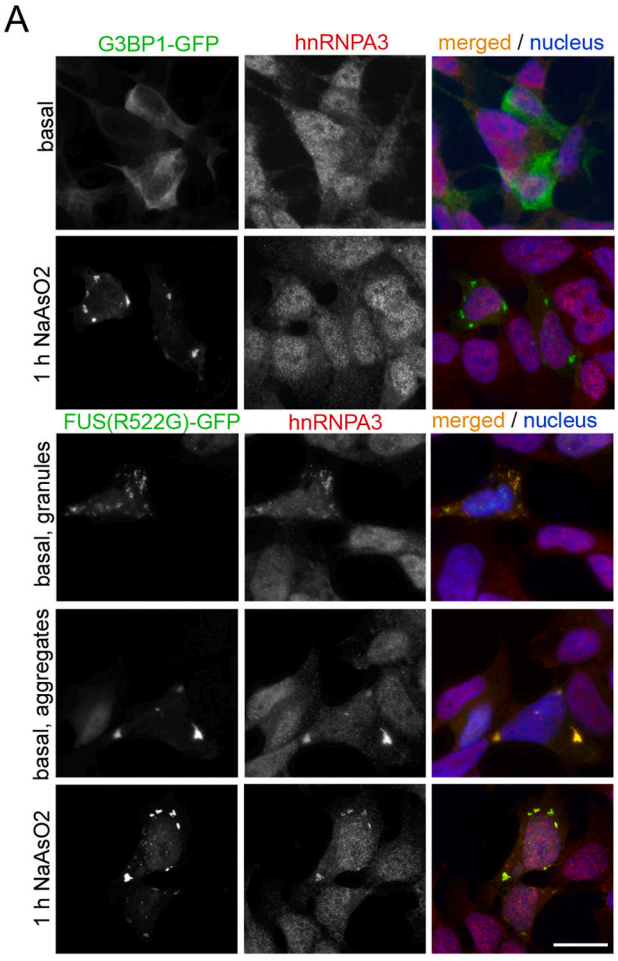

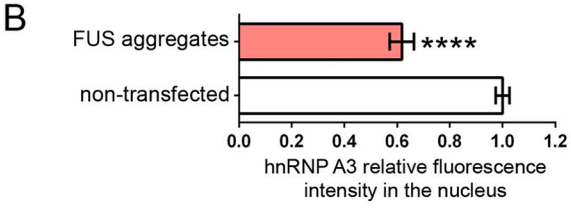

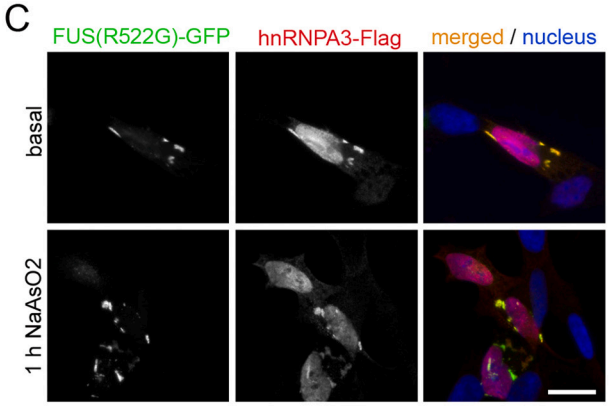

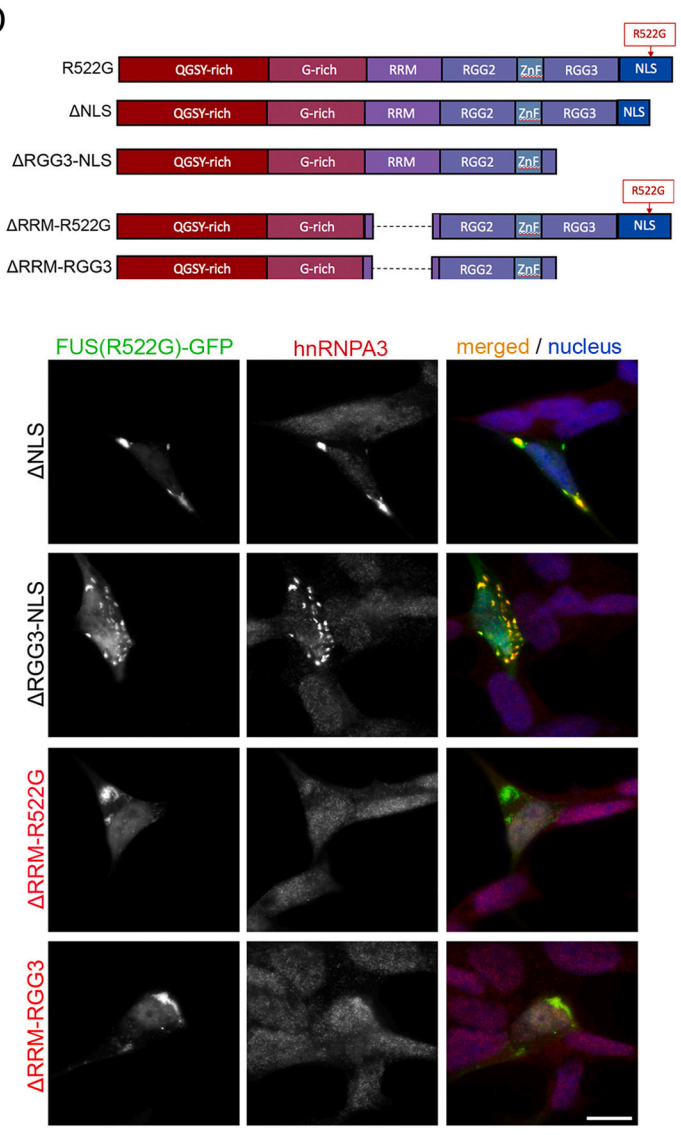

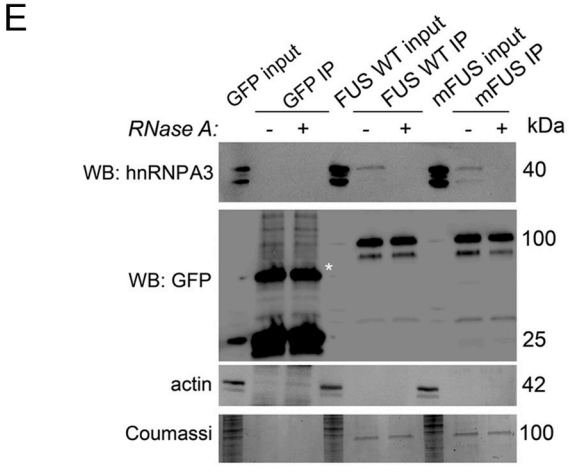

(caption on next page)

Fig. 4. hnRNPA3 interacts with FUS and is recruited into FUS aggregates in an RNA-dependent manner.
(A) Enrichment of endogenous hnRNPA3 in FUS granules and their clusters in unstressed cells and in mFAs in stressed cells, but not in SGs formed by G3BP1-GFP. SH-SY5Y cells transiently expressing FUS(R522G)-GFP or G3BP1-GFP were immunostained with an anti-hnRNPA3 antibody 24 h post-transfection. Unstressed cells with FUS granules and their clusters (FUS aggregates) as well as $NaAsO_2$ treated cells are shown. Scale bar, 10 μm.
(B) hnRNPA3 depletion from the nucleus of cells containing FUS aggregates. Cells transiently expressing FUS(R522G)-GFP were immunostained with an anti-hnRNPA3 antibody 24 h post-transfection. Intensity of hnRNPA3 fluorescence signal in the nucleus was measured in cells containing compact FUS aggregates ($n = 12$) and adjacent non-transfected cells ($n = 24$). Error bars represent S.E.M. ****$p < 0.0001$ (two-tailed Student's *t*-test).
(C) Co-localization of transiently expressed FUS(R522G)-GFP and hnRNPA3-Flag in FUS aggregates and $NaAsO_2$-induced mFAs in SH-SY5Y cells. Scale bar, 10 μm.
(D) Mapping of FUS domains required for hnRNPA3 recruitment into FUS aggregates. SH-SY5Y cells were analyzed 24 h post-transfection with the respective deletion construct, by anti-hnRNPA3 staining. FUS deletion mutants deficient in hnRNPA3 sequestration are given in red. Scale bar, 10 μm.
(E) Co-IP of endogenous hnRNPA3 by GFP-tagged WT or mutant (R522G) FUS (mFUS) from overexpressing HEK293 cells. Lysates of cells expressing GFP, FUS WT and mutant FUS were treated with RNase A or left untreated under the same conditions and GFP-tagged proteins were precipitated using GFP-Trap® beads. Input is 10% of the final IP fraction. Asterisk indicates a non-specific band in "GFP only" pull-downs.

granules/aggregates in unstressed cells, these structures are highly dynamic therefore might not tightly capture and trap the protein and therefore might not elicit its loss of function. We reported previously that prolonged exposure of cells with FUS aggregates to a transcription blocker actinomycin D leads to their conversion into RNA-free and presumably more stable structures (Shelkovnikova et al., 2014a). We also found that chemical inhibition of the proteasome leads to the formation of large, 1–2 per cell aggregates in FUS(R522G)-GFP expressing cells (Fig. 5A) which likely correspond to aggresomes (An and Statsyuk, 2015). These two types of aggregates seemingly better mimic pathological, stable FUS inclusions typical for ALS-FUS than the dynamic mFAs. We examined hnRNPA3 association with the structures induced by either a 6-h actinomycin D treatment or a 8-h MG132 treatment. Strikingly, hnRNPA3 was found condensed within the single, largest cytoplasmic FUS aggregate and depleted from the surrounding smaller aggregates in MG132-treated cells (Fig. 5A). Likewise, hnRNPA3 was highly concentrated within RNA-free FUS aggregates in actinomycin D treated cells (Fig. 5A).

We next examined the presence of hnRNPA3 in neuronal mutant FUS inclusions in a transgenic mouse model of FUS proteinopathy (Shelkovnikova et al., 2013a). These mice express a truncated version of FUS lacking RGG boxes and ZnF domain and therefore were not expected to efficiently interact with hnRNPA3 (Fig. 5D). However inclusions formed by this variant also sequester normal endogenous FUS (Shelkovnikova et al., 2013a; Shelkovnikova et al., 2013b) that may piggy-back hnRNPA3 into these structures. Immunostaining of the spinal cord tissue from symptomatic 4-month old mice showed accumulation of hnRNPA3 in a form of cytoplasmic and nuclear inclusions in neurons of transgenic mice, whereas WT mice displayed only normal nuclear hnRNPA3 staining (Fig. 5B).

Thus hnRNPA3 protein is sequestered into dynamic mFAs via RNA-dependent interactions but is also highly accumulated in stable FUS inclusions.

2.5. *Downregulation of the Drosophila ortholog is deleterious and exacerbates FUS toxicity*

Sequestration of hnRNPA3 into FUS aggregates/inclusions may lead to its loss of function. hnRNPA3 function in mammals is poorly characterized, so far the protein has been implicated in DNA damage response (Nihei et al., 2020) and RNA trafficking by RNP granules (Ma et al., 2002), although associated molecular mechanisms remain unclear. We therefore decided to examine the consequences of hnRNPA3 loss of function in vivo, including in the context of FUS proteinopathy. We generated transgenic *Drosophila* with silenced retinal expression of the fly hnRNPA3 ortholog, Hrb87F, and crossed this line with FUS transgenic flies. *Drosophila* lines with retinal overexpression of human wild-type (WT) FUS were described previously (Matsukawa et al., 2021; Matsumoto et al., 2018); they are characterized by a marked retinal thinning (~30% reduced retinal thickness) (Fig. 6A, B). RNAi of Hrb87F on its own resulted in retinal degeneration, comparable in its severity with the changes caused by human FUS overexpression (Fig. 6A, B), pointing to an important housekeeping role of the hnRNPA3 ortholog in flies. In double transgenic flies, retinal degeneration was significantly more pronounced than in FUS WT or Hrb87F-RNAi flies, with almost complete loss of ommatidia (Fig. 6A, B). This result is indicative of additive toxicity of FUS accumulation and loss of Hrb87F expression. It should be noted that human FUS levels were reduced in the retinas of double transgenic flies as measured by western blot (Fig. 6C), which may be attributed by significant retinal thinning in these flies or regulation of FUS levels by Hrb87F protein. Thus, loss of function of hnRNPA3 ortholog is deleterious and synergizes with FUS toxicity in flies.

3. Discussion

In the current report, we provide proteomic evidence, backed by cellular and in vivo validation studies, that: *i)* mutant FUS enriched cytoplasmic assemblies formed in stressed cells are compositionally distinct from physiological SGs and cannot fully replace them functionally; *ii)* presence of cytoplasmic FUS assemblies is expected to negatively affect multiple cellular pathways; *iii)* composition of mutant FUS assemblies may promote their persistence. Our data strongly support a pathological role for stress-induced FUS aggregation in the cytoplasm in ALS-FUS, realized via its negative impact on normal SG functions and gain of novel unwanted functions by such aggregates.

Our analysis of SGs and mFAs purified in parallel revealed that a certain "core" network of proteins related to the RNP granule assembly, regulation of protein translation, RNA metabolism and gene expression are still recruited into FUS-containing RNP granules during stress. However FUS assemblies share only one-third of their proteome with SGs and are significantly depleted of signal transduction proteins typically recruited by normal SGs. Therefore, although mFAs may adopt some functions typical for physiological SGs, the full functional replacement of SGs by FUS assemblies, especially related to SG role in stress signaling, is hardly possible. Importantly, since we detected a set of proteins depleted from the proteome of mFAs as compared to SGs, it can be concluded that not only collections of FUS granules but also FUS-containing SGs (formed in cells with diffuse cytoplasmic FUS localization pre-stress) are structurally different from normal SGs.

While strong experimental evidence supports the role of cytoplasmic gain of FUS function in ALS-FUS pathogenesis (Devoy et al., 2017; Scekic-Zahirovic et al., 2016; Sharma et al., 2016), the contribution of cytoplasmic FUS aggregation to the pathology development remained largely unaddressed. In two recent reports, phase-separated/aggregated FUS species from human or mouse cells were captured and proteomically profiled (Kamelgarn et al., 2018; Reber et al., 2021). These studies identified the major cellular pathways modulated by aggregated FUS, most notably splicing, protein translation, nonsense-mediated mRNA decay and mitochondrial homeostasis. Mutant FUS was found to be disruptive for cellular processes as compared to WT protein, and FUS toxicity can be at least partially dependent of its ability to phase-separate. FUS phase separation and aggregation, including partitioning into SGs, is dramatically enhanced by stress, and external stresses are believed to play a role as secondary triggers, or second hits, in ALS-FUS

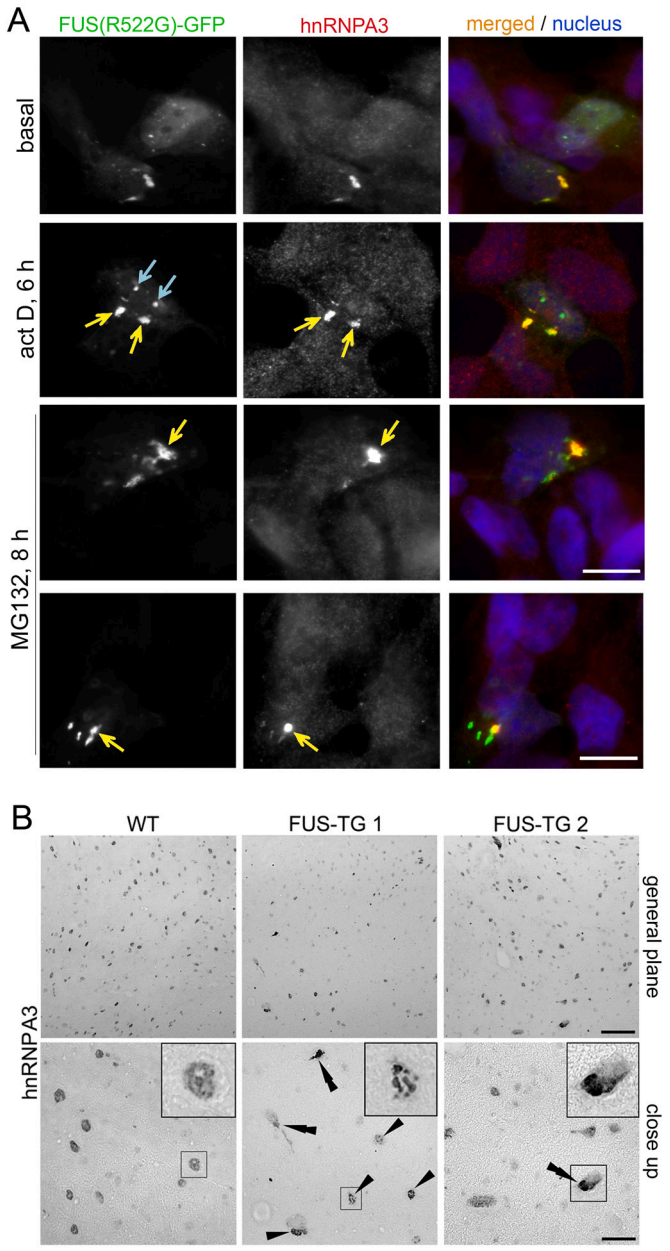

Fig. 5. hnRNPA3 recruitment into FUS inclusions in cultured cells and in transgenic mice.
(A) hnRNPA3 recruitment into stable FUS aggregates in cells subjected to a transcription or proteasome inhibitor. Cells expressing FUS(R522G)-GFP were treated with MG132 for 8 h or actinomycin D for 6 h. hnRNPA3-positive inclusions are indicated with yellow arrows. Note FUS-positive nucleolar caps typically formed in actinomycin D treated cells (blue arrows). Scale bar, 10 μm. (B) Immunostaining of the spinal cord sections of WT and FUS-TG mice. Images for a 4-month old WT mouse and two symptomatic FUS-TG mice are shown. Nuclear inclusions are indicated with single arrowheads and cytoplasmic inclusions - with double arrowheads. Scale bars, 100 μm and 20 μm for general plane and magnified images, respectively.

development (Al-Chalabi et al., 2014; Dormann et al., 2010; Shelkovnikova et al., 2019). FUS assemblies, often referred to as 'pathological SGs', were reported to recruit some factors not normally present in physiological SGs, for example components of P-bodies, paraspeckles and the spliceosome (Gerbino et al., 2013; Shelkovnikova et al., 2014a; Shelkovnikova et al., 2014b). However until now, global molecular differences and similarities between these two types of RNP granules remained uncharacterized. We adopted an approach different from the published studies – a parallel affinity purification of these two stress-induced granules – that allowed direct comparisons. A relatively small proportion of proteins from both published interactomes of aggregated FUS (26% and 18% for human and mouse cells, respectively) (Kamelgarn et al., 2018; Reber et al., 2021) was found in our mFA core proteome. This is likely due to a principally different approach to aggregated FUS isolation (intact stable cores vs. aggregated species from cell lysates) but also the use of stressed cells in our study. Indeed, it is known that protein networks undergo significant remodeling during stress (Markmiller et al., 2018; Youn et al., 2018). It should be also noted that the protocol used here excluded the "shell" proteins surrounding mFA cores. For example, TIAR and G3BP1 are not FUS granule components yet they are incorporated in FUS aggregates, as has been demonstrated using high-resolution imaging (Shelkovnikova et al., 2019).

We found that several classes of proteins are abnormally enriched in mFAs, as compared to SGs, namely mitochondrial proteins, translation and mRNA surveillance pathway factors, and components of the spliceosome, in full agreement with the above proteomic studies (Kamelgarn et al., 2018; Reber et al., 2021) and several functional studies. In particular, FUS was shown to interact with mitochondria (Deng et al., 2015), and mutant FUS was proven to have a negative effect on translation (Lopez-Erauskin et al., 2018; Scekic-Zahirovic et al., 2016; Yasuda et al., 2013). Mislocalization/dysregulation of spliceosome subunits and disruption of nuclear SMN-containing RNP granules, Gems, in mutant FUS expressing cells is a well-established phenotype (Gerbino et al., 2013; Reber et al., 2016; Yamazaki et al., 2012). Interestingly, spliceosome and mRNA surveillance factors DAZAP1 and CPSF6 sequestered into mFAs are also the components of nuclear RNP granules paraspeckles. DAZAP1 is a core paraspeckle protein responsible for the stability of this granule, whereas loss of CPSF6 function is known to lead to enhanced accumulation of the structural paraspeckle RNA, NEAT1_2 (Naganuma et al., 2012). Indeed, recently we demonstrated that paraspeckle integrity is affected in cells expressing mutant FUS despite accumulation of NEAT1_2 (An et al., 2019a).

Although generally the same pathways are disrupted via protein sequestration by aggregated FUS in unstressed and stressed cells, our approach revealed that certain pathways may become dysregulated specifically under stress conditions due to the exclusion of some proteins from mFAs. In addition to the low recruitment of signal transduction proteins into mFA cores as described above, NPC proteins were found depleted from mFA cores as compared to SG cores. Redistribution of nucleocytoplasmic transport factors into SGs is likely an important aspect of cellular stress response, which when dysregulated, can contribute to ALS pathology (Zhang et al., 2018). Further, we found that mFAs are depleted of proteasome subunits as compared to normal SGs. Recently, 26S proteasome was shown to be recruited into arsenite-induced SGs to enable their clearance post-stress, whereas impaired proteasome function can lead to SG transformation into aberrant structures that require autophagic clearance (Turakhiya et al., 2018). SGs were also shown to recruit sumoylation factors which facilitate their disassembly, and these factors were depleted from SGs in cells accumulating C9ORF72 pathological dipeptides (Marmor-Kollet et al., 2020). In agreement with this data, SUMO1 and SUMO2 were detected in SG cores but not mFA cores in our study. Strikingly, we also found that mFAs are characterized by significantly more extensive network of physical interactions between their protein components, as compared to SGs. Indeed, proteins within mFA cores have, on average, twice as many physical interactors as the proteins in SG cores. Tighter connections between mFA components coupled with inefficient recruitment of disassembly proteins may contribute to their deficient clearance, persistence and subsequent conversion into pathological inclusions. Notably, while SGs form in cells only in response to acute stress, FUS aggregates can form spontaneously and persist for prolonged periods of time (Shelkovnikova et al., 2019). They therefore can induce a stress-mimicking state in neurons by retention of proteins (and RNAs)

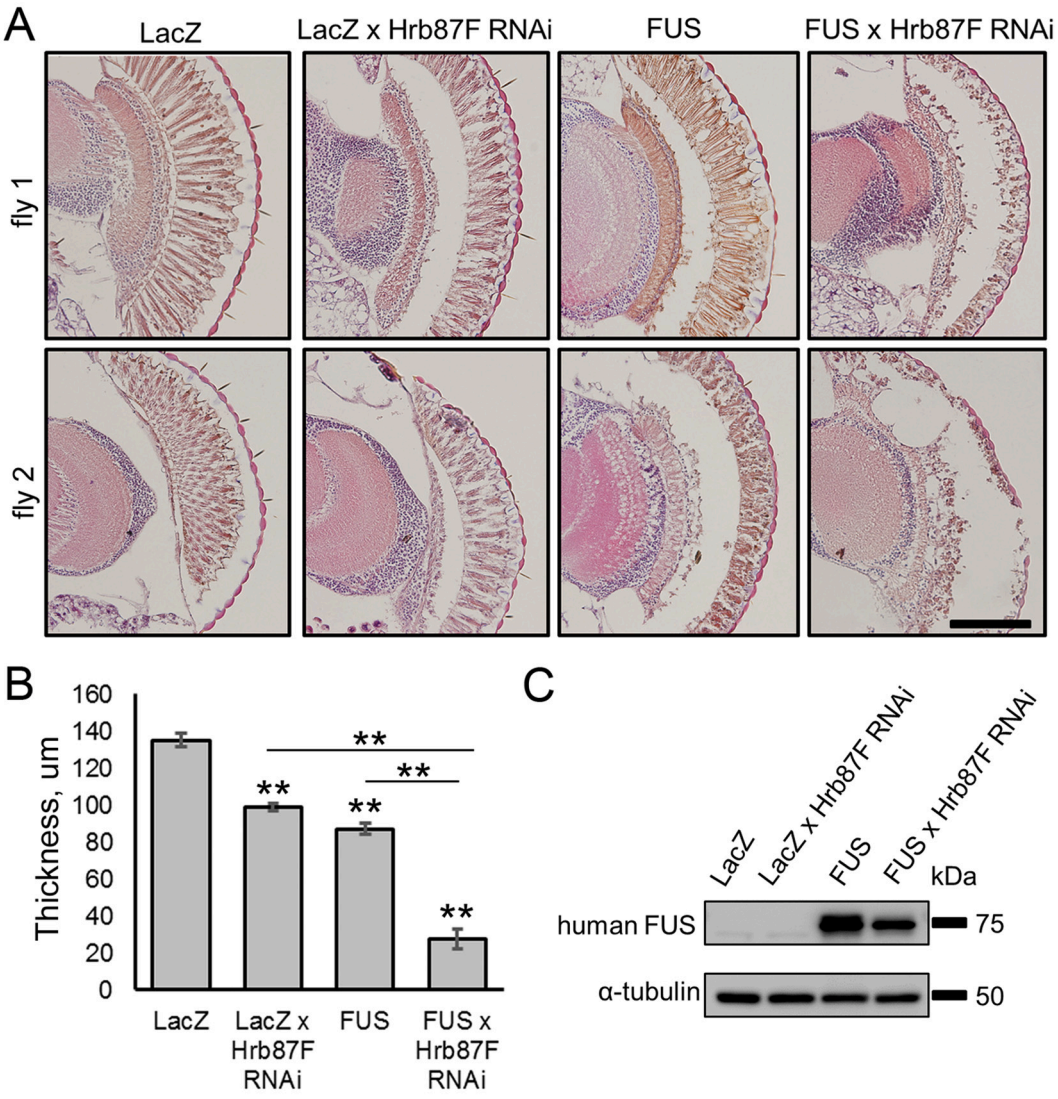

Fig. 6. Depletion of the *Drosophila* hnRNPA3 ortholog causes retinal degeneration and exacerbates toxicity of human FUS in the retina.
(A, B) Downregulation of Hrb87F, the fly ortholog of human hnRNPA3, using RNAi, leads to retinal thinning and aggravates FUS WT toxicity in transgenic *Drosophila*. Representative images of retinal sections (A) and quantification of retinal thickness (B) are shown. In B, $n = 10$ for each genotype, error bars represent S.E.M. $^{**}p < 0.01$ (one-way ANOVA with post-hoc Tukey-Krammer test). Scale bar, 100 μm.
(C) Levels of human FUS WT in the *Drosophila* retina in single and double (FUS/Hrb87F) transgenic flies. A representative western blot is shown.

normally sequestered into SGs. This "preconditioned", chronic stress state might render neurons more vulnerable to a subsequent acute stress (Shelkovnikova et al., 2017).

We found that hnRNPA3, a protein recruited into mFAs and also into FUS granule clusters in unstressed cells, but not SGs, remains associated with RNA-free FUS aggregates induced by transcription inhibition and is highly concentrated in aggresome-like structures in cells with inhibited proteasome function. Such aggregates likely better mimic pathological inclusions seen in ALS-FUS, and consistent with this, we detected hnRNPA3 in neuronal FUS inclusions in transgenic mice. In FUS aggregate-containing cells, reduced nuclear levels hnRNPA3 were also observed. Deleterious effect of hnRNPA3 loss of function in vivo was confirmed by silencing its ortholog, Hrb87F, in the *Drosophila* retina. Previously, loss of hnRNPA3 function downstream ALS-C9 pathology leading to DNA damage response deficiencies was reported (Mori et al., 2013; Nihei et al., 2020). Mutant FUS is known to cause DNA damage via a number of mechanisms (Sukhanova et al., 2020) therefore more in-depth studies are required to establish whether hnRNPA3 loss of function via FUS aggregate entrapment mediates some of these as well as other ALS-FUS mechanisms. We found that the toxicities of FUS overexpression and Hrb87F loss synergize to cause a more severe degenerative phenotype in flies, establishing hnRNPA3 as a protein with possible protective effect in ALS-FUS. Consistent with a negative effect of Hrb87F downregulation identified in tour study, neuronal Hrb87F silencing was previously found to cause locomotion defects in flies (Appocher et al., 2017). However in a TDP-43 fly model, Hrb87F depletion provided partial rescue of TDP-43 toxicity (Appocher et al., 2017). hnRNPA3 was also detected among significantly downregulated proteins in human cells after TDP-43 knockdown (Prpar Mihevc et al., 2016). Thus hnRNPA3 may play a differential role in ALS-FUS and in ALS with TDP-43 pathology.

In conclusion, our results suggest that comparative analysis of physiological SGs and their abnormal counterparts formed in cells expressing ALS mutants under stress can identify novel pathologically relevant pathways/factors and determinants of insoluble inclusion formation in ALS subtypes.

4. Materials and methods

4.1. Cell culture and maintenance

HEK293 and SH-SY5Y cells were maintained in DMEM/F12 medium supplemented with 10% foetal bovine serum (FBS), penicillin-streptomycin and GlutaMAX® (all Invitrogen). Production of plasmids encoding G3BP1-GFP (pEGFP-N1 vector), FUS(R522G)-GFP (pEGFP-C1 vector) and FUS deletion mutants is described in our previous studies (An et al., 2019b; Shelkovnikova et al., 2014a). Plasmid for the expression of Flag-tagged hnRNPA3 was purchased from Sino Biological (Cat #CG90366-NF-SIB). For small-scale transfections in cellular validation analysis, Lipofectamine2000 (Invitrogen) was used in 24-well plates. Cells were treated with 0.5 mM $NaAsO_2$ (sodium arsenite) for 1 h to induce SG and mFA assembly; for 8 h with 10 μM MG132 or for 6 h with 5 μM actinomycin D to induce larger/stable FUS aggregates (all compounds purchased from Sigma).

4.2. Affinity purification of SG and mFA cores

SG and mFA cores were purified from HEK293 cells transiently expressing G3BP1-GFP or FUS(R522G)-GFP according to a previously published protocol, with modifications (Jain et al., 2016; Wheeler et al., 2017). HEK293 cells were transfected with plasmids to express GFP alone, G3BP1-GFP and FUS(R522G)-GFP in 6-cm dishes (1 μg plasmid/dish) using Lipofectamine2000. The following day (~24 h post-transfection), cells were treated with 0.5 mM $NaAsO_2$ for 1 h, snap-frozen on dishes and processed for SG/mFA core purification in parallel. Cells were scraped in the lysis buffer containing 50 mM TrisHCl pH 7.4, 100 mM KOAc, 2 mM MgOAc, 0.5 mM DTT, 50 μg/ml heparin, 0.5% NP-40 and supplemented with RNase inhibitor (Murine, M0314, New England Biolabls) and protease inhibitors cocktail (cOmplete Mini, Roche), and passed through a 25G needle 7 times. Lysates were left on ice for 15 min with periodic vortexing. Lysates were subsequently centrifuged at 1000 ×*g* for 5 min, and the supernatant was centrifuged again at 17,000 ×*g* for 20 min, to pellet the cores. The pellets washed twice in the lysis buffer, resuspended in the same buffer and incubated with GFP-Trap® agarose beads for 4 h. Beads were washed three times with washing buffer 1 (20 mM TrisHCl, 200 mM NaCl, pH 8.0) and once with washing buffer 2 (20 mM TrisHCl, 500 mM NaCl, pH 8.0) and once with washing buffer 3 (lysis buffer supplemented with 2 M urea). Resultant bead slurry was used for proteomic (LC-MS/MS) analysis. Purification of SG and mFA cores was performed in duplicates and twice, on two different days, and proteomic analysis was done on two samples (combination of two biological replicates each, $n = 4$) per condition.

4.3. Proteomic analysis

Proteomic analysis was performed at the Bristol Proteomics Facility as described in (An et al., 2019b). Peptide data were filtered to satisfy false discovery rate (FDR) of 1%. Peptides identified were mapped to proteins using the respective tool of the UniProt online database (https://www.uniprot.org/). Proteins identified in the samples from cells expressing GFP alone were used as a background list and were subsequently subtracted from final SG and mFA core protein lists. Venn diagrams were prepared using BioVenn online tool (http://www.biovenn.nl/index.php) (Hulsen et al., 2008). Protein networks were prepared using the STRING Database v.11.5 (https://string-db.org/). Enrichment analysis was carried out using Enrichr (https://amp.pharm.mssm.edu/Enrichr/) (Chen et al., 2013; Kuleshov et al., 2016) and Revigo (http://revigo.irb.hr/) (Supek et al., 2011) online tools.

4.4. RNA analysis

RNA was purified from cell lysates (total cellular RNA) and separately from SG and mFA core fractions using TRI-reagent (Sigma). Total RNA was approximately 10 times more concentrated than RNA from SG/mFA core fractions (~100 ng/μl vs. 10 ng/μl) and therefore was diluted accordingly prior to analysis. cDNA synthesis was performed using random primers (Promega) and M-MLV reverse transcriptase (Promega), according to manufacturer's instructions. Non-saturated PCR (26 cycles) was performed using New England BioLabs Taq DNA polymerase (M0273). Primer sequences were: CHD7: 5'-GCAGAAAGTGCCTGTGCATC-3′ and 5'-GCTGAGCATTCGGTCCACTA-3′; BCL9L: 5'-CGTACAGTGGGGACGAATGG-3′ and 5'-ATGGCTGGGTCTGCTACATT-3′; UBL5: 5'-CTGATTGCAGCCCAAACTGG-3′ and 5'-CAGGTTCATCCCATCGTGGA-3′; MACF1: 5'-TGCATGAGCAGAAAAAGCGG-3′; 5'-TTTCTTCTGAACCCGGTCCC-3′; RPL39: 5'-GTGTGTTCTTGACTCCGCTG-3′ and 5'-TTCATCCGAATCCACTGGGG-3′; GAPDH: 5'-TCGCCAGCCGAGCCA-3′ and GAGTTAAAAGCAGCCCTGGTG-3′; MAPT: 3'-ACACGGAGATCCCAGAAGGA-3′ and 5'-CCACTTTCAGGCTCTTGGGT-3′; TIA1: 5'-TTGGGAGGTAGTGAAGGGCA-3′ and 5'-TGGAAAGGTTACCGACGTATAGAG-3′; NVL: 5'-GGCGAAGGCTGTTGCAAAT-3′ and 5'-AAAACTTGTCGCACAGCACG-3′; TAF15: 5'-GGCGTGGGGGATATGACAAG-3′ and 5'-TCCATAATCCCTGTGACCACC-3′.

4.5. Immunocytochemistry

Immunocytochemistry and microscopic analysis were performed as described earlier (Kukharsky et al., 2015), with modifications. Briefly, HEK293 or SH-SY5Y cells were plated on uncoated coverslips, transfected and stressed 24 h post-transfection. Cells were fixed in 4% paraformaldehyde for 15 min at RT and permeabilized for 5 min in cold methanol. Primary antibodies in blocking solution (5% goat serum in 0.1% Triton-X100/1xPBS) were applied for 2 h at RT or, when needed, overnight at 4 °C. Secondary Alexa488- or Alexa546-conjugated antibodies (Molecular Probes) separately or in cocktail were added for 1 h at RT. Nuclei were visualized with a 5-min incubation in 10 μg/ml DAPI solution (Sigma). Fluorescent images were taken with 100× objective (UPlanFI 100×/1.30) on BX57 fluorescent microscope equipped with ORCA-Flash 4.0 camera (Hamamatsu) and cellSens Dimension software (Olympus). Figures were prepared using Photoshop CS3 or PowerPoint 2016 software. hnRNPA3 depletion from the nucleus was quantified by measuring the fluorescence intensity in a 50 × 50 pixel square in the nuclei of FUS aggregate-containing and non-transfected cells using the free Image J software https://imagej.nih.gov/ij/.

4.6. Immunoprecipitation (IP) and western blotting

Cells were washed with PBS, lysed in ice cold IP buffer (1% Triton-X100 in PBS) on ice with periodic vortexing for 15 min. Unbroken cells and cell debris were pelleted at 17,000 ×g for 15 min, and input samples were taken at this point. Cleared cell lysates were split in half and one half was treated with RNase A (100 μg/ml) for 30 min at RT. Lysates were then incubated with GFP-Trap® agarose beads (Chromo-Tek) for 4 h at 4 °C. Beads were washed four times with ice cold IP buffer, and bound protein complexes were eluted by heating the samples for 10 min at 95 °C in 2xLaemmli loading buffer. Pull-down efficiency was analyzed by western blot. For input, 10% of the final IP sample was loaded on the gel. Proteins were resolved in Mini-Protean® TGX precast gels (Bio-Rad) and transferred to the PVDF membrane (GE Healthcare) by semi-dry blotting. Membranes were blocked in non-fat 4% milk in TBS/T and incubated with primary and HRP-conjugated secondary (GE Healthcare) antibodies. For signal detection, Clarity Max ECL kit and ChemiDoc™ Gel Imaging System (Bio-Rad) were used.

4.7. Primary antibodies

The following commercial primary antibodies were used: hnRNPA3 (rabbit polyclonal, 25142–1-AP, Proteintech); CPSF6 (rabbit polyclonal, A301-356A, Bethyl); NCBP1 (rabbit polyclonal, 10349–1-AP,

Proteintech); DAZAP1 (rabbit polyclonal, A303-984A, Bethyl); EXOSC3 (rabbit polyclonal, 15062–1-AP, Proteintech); SAFB (rabbit polyclonal, 21857–1-AP, Proteintech); GFP (mouse monoclonal, sc-9996, Santa Cruz); Flag (DYKDDDDK Tag, mouse monoclonal, 9A3, Cell Signaling); beta-actin (mouse monoclonal, A5441, Sigma). Antibodies were used at 1:1,000 dilution for immunostaining and western blot.

4.8. Immunohistochemistry on mouse samples

Spinal cord sections (8 μm thick) from wild-type and 4-month old symptomatic FUS-TG mice (Shelkovnikova et al., 2013a) were used. After rehydration, sections were subjected to microwave antigen retrieval in sodium citrate buffer (pH 6.0) and blocked using 10% goat serum in PBS/T. Sections were incubated with the primary anti-hnRNPA3 antibody (Proteintech, 25142–1-AP) overnight at 4 °C and secondary HRP-conjugated anti-rabbit IgG antibody (Vector Laboratories) for 1.5 h at RT. Signal was detected using Vectastain® Elite ABC Universal Plus Kit (Vector Laboratories) and 3,3′-diaminobenzidine (DAB, Sigma). Images were taken using BX57 microscope (Olympus) and ORCA-Flash 4.0 camera (Hamamatsu).

4.9. Generation and analysis of transgenic Drosophila

Generation of *Drosophila* lines with human retinal expression of FUS WT is described elsewhere (Matsumoto et al., 2018). gmr-GAL4, UAS-lacZ and Hrb87F RNAi lines were obtained from the Bloomington Drosophila stock centre. For histochemical analysis, heads of 5-day-old adult flies were dissected, briefly washed in PBS and fixed with 4% PFA containing 0.1% Triton X-100 at RT for 2 h. After brief wash in PBS, tissues were dehydrated by graded ethanol, cleared in butanol and embedded in paraffin. Four-micrometre thick coronal sections were stained with hematoxylin and eosin (H&E). Ten animals of each genotype were used for retinal thickness quantification. For western blot analysis, heads of 5-day-old flies were dissected and lysed in Laemmli sample buffer for SDS-PAGE. Bethyl (A300-293A) anti-FUS antibody was used for western blot.

Declaration of Competing Interest

Authors declare no competing interests.

Acknowledgements

We thank Bristol Proteomics Facility for their help with proteomic analysis. The study was supported by fellowships from Medical Research Foundation and Motor Neurone Disease Association (Shelkovnikova/Oct17/968-799) to TAS. HA was a recipient of Cardiff University/China Scholarship Council PhD studentship and GL – IAESTE studentship.

Appendix A. Supplementary data

Supplementary data to this article can be found online at https://doi.org/10.1016/j.nbd.2021.105585.

References

Al-Chalabi, A., et al., 2014. Analysis of amyotrophic lateral sclerosis as a multistep process: a population-based modelling study. The Lancet. Neurology. 13, 1108–1113.
An, H., Statsyuk, A.V., 2015. An inhibitor of ubiquitin conjugation and aggresome formation. Chem. Sci. 6, 5235–5245.
An, H., et al., 2019a. ALS-linked FUS mutations confer loss and gain of function in the nucleus by promoting excessive formation of dysfunctional paraspeckles. Acta neuropathologica communications. 7, 7.
An, H., et al., 2019b. Stress granules regulate stress-induced paraspeckle assembly. J. Cell Biol. 218, 4127–4140.
Appocher, C., et al., 2017. Major hnRNP proteins act as general TDP-43 functional modifiers both in Drosophila and human neuronal cells. Nucleic Acids Res. 45, 8026–8045.
Aulas, A., Vande Velde, C., 2015. Alterations in stress granule dynamics driven by TDP-43 and FUS: a link to pathological inclusions in ALS? Front. Cell. Neurosci. 9, 423.
Baron, D.M., et al., 2013. Amyotrophic lateral sclerosis-linked FUS/TLS alters stress granule assembly and dynamics. Mol. Neurodegener. 8, 30.
Blokhuis, A.M., et al., 2016. Comparative interactomics analysis of different ALS-associated proteins identifies converging molecular pathways. Acta Neuropathol. 132, 175–196.
Bosco, D.A., et al., 2010. Mutant FUS proteins that cause amyotrophic lateral sclerosis incorporate into stress granules. Hum. Mol. Genet. 19, 4160–4175.
Chen, E.Y., et al., 2013. Enrichr: interactive and collaborative HTML5 gene list enrichment analysis tool. BMC bioinformatics. 14, 128.
Deng, J., et al., 2015. FUS interacts with HSP60 to promote mitochondrial damage. PLoS Genet. 11, e1005357.
Devoy, A., et al., 2017. Humanized mutant FUS drives progressive motor neuron degeneration without aggregation in 'FUSDelta14' knockin mice. Brain J. Neurol. 140, 2797–2805.
Dormann, D., et al., 2010. ALS-associated fused in sarcoma (FUS) mutations disrupt Transportin-mediated nuclear import. EMBO J. 29, 2841–2857.
Gerbino, V., et al., 2013. Mislocalised FUS mutants stall spliceosomal snRNPs in the cytoplasm. Neurobiol. Dis. 55, 120–128.
Hardiman, O., et al., 2017. Amyotrophic lateral sclerosis. Nature reviews. Disease primers. 3, 17085.
Hulsen, T., et al., 2008. BioVenn - a web application for the comparison and visualization of biological lists using area-proportional Venn diagrams. BMC Genomics 9, 488.
Jain, S., et al., 2016. ATPase-modulated stress granules contain a diverse proteome and substructure. Cell. 164, 487–498.
Japtok, J., et al., 2015. Stepwise acquirement of hallmark neuropathology in FUS-ALS iPSC models depends on mutation type and neuronal aging. Neurobiol. Dis. 82, 420–429.
Kamelgarn, M., et al., 2018. ALS mutations of FUS suppress protein translation and disrupt the regulation of nonsense-mediated decay. Proc. Natl. Acad. Sci. U. S. A. 115, E11904–E11913.
Kedersha, N., Anderson, P., 2002. Stress granules: sites of mRNA triage that regulate mRNA stability and translatability. Biochem. Soc. Trans. 30, 963–969.
Kedersha, N., et al., 2013. Stress granules and cell signaling: more than just a passing phase? Trends Biochem. Sci. 38, 494–506.
Khong, A., et al., 2017. The stress granule transcriptome reveals principles of mRNA accumulation in stress granules. Mol. Cell 68 (808–820), e5.
Kino, Y., et al., 2015. FUS/TLS deficiency causes behavioral and pathological abnormalities distinct from amyotrophic lateral sclerosis. Acta Neuropathologica Communications 3, 24.
Kukharsky, M.S., et al., 2015. Calcium-responsive transactivator (CREST) protein shares a set of structural and functional traits with other proteins associated with amyotrophic lateral sclerosis. Mol. Neurodegener. 10, 20.
Kuleshov, M.V., et al., 2016. Enrichr: a comprehensive gene set enrichment analysis web server 2016 update. Nucleic Acids Res. 44, W90–W97.
Kwiatkowski Jr., T.J., et al., 2009. Mutations in the FUS/TLS gene on chromosome 16 cause familial amyotrophic lateral sclerosis. Science. 323, 1205–1208.
Lagier-Tourenne, C., et al., 2012. Divergent roles of ALS-linked proteins FUS/TLS and TDP-43 intersect in processing long pre-mRNAs. Nat. Neurosci. 15, 1488–1497.
Lattante, S., et al., 2013. TARDBP and FUS mutations associated with amyotrophic lateral sclerosis: summary and update. Hum. Mutat. 34, 812–826.
Li, Y.R., et al., 2013. Stress granules as crucibles of ALS pathogenesis. J. Cell Biol. 201, 361–372.
Lopez-Erauskin, J., et al., 2018. ALS/FTD-linked mutation in FUS suppresses intra-axonal protein synthesis and drives disease without nuclear loss-of-function of FUS. Neuron 100, 816–830.
Ma, A.S., et al., 2002. Heterogeneous nuclear ribonucleoprotein A3, a novel RNA trafficking response element-binding protein. J. Biol. Chem. 277, 18010–18020.
Mackenzie, I.R.A., et al., 2010. TDP-43 and FUS in amyotrophic lateral sclerosis and frontotemporal dementia. Lancet Neurol. 9, 995–1007.
Markmiller, S., et al., 2018. Context-dependent and disease-specific diversity in protein interactions within stress granules. Cell. 172 (590–604), e13.
Marmor-Kollet, H., et al., 2020. Spatiotemporal proteomic analysis of stress granule disassembly using APEX reveals regulation by SUMOylation and links to ALS pathogenesis. Mol. Cell 80 (876–891), e6.
Matsukawa, K., et al., 2021. Long non-coding RNA NEAT1_1 ameliorates TDP-43 toxicity in in vivo models of TDP-43 proteinopathy. RNA Biol. 1–9.
Matsumoto, T., et al., 2018. Self-assembly of FUS through its low-complexity domain contributes to neurodegeneration. Hum. Mol. Genet. 27, 1353–1365.
Mori, K., et al., 2013. hnRNP A3 binds to GGGGCC repeats and is a constituent of p62-positive/TDP43-negative inclusions in the hippocampus of patients with C9orf72 mutations. Acta Neuropathol. 125, 413–423.
Naganuma, T., et al., 2012. Alternative 3′-end processing of long noncoding RNA initiates construction of nuclear paraspeckles. EMBO J. 31, 4020–4034.
Nihei, Y., et al., 2020. Poly-glycine-alanine exacerbates C9orf72 repeat expansion-mediated DNA damage via sequestration of phosphorylated ATM and loss of nuclear hnRNPA3. Acta Neuropathol. 139, 99–118.
Prpar Mihevc, S., et al., 2016. TDP-43 aggregation mirrors TDP-43 knockdown, affecting the expression levels of a common set of proteins. Sci. Rep. 6, 33996.
Reber, S., et al., 2016. Minor intron splicing is regulated by FUS and affected by ALS-associated FUS mutants. EMBO J. 35, 1504–1521.
Reber, S., et al., 2021. The phase separation-dependent FUS interactome reveals nuclear and cytoplasmic function of liquid-liquid phase separation. Nucleic Acids Res. 49, 7713–7731.

Scekic-Zahirovic, J., et al., 2016. Toxic gain of function from mutant FUS protein is crucial to trigger cell autonomous motor neuron loss. EMBO J. 35, 1077–1097.
Sharma, A., et al., 2016. ALS-associated mutant FUS induces selective motor neuron degeneration through toxic gain of function. Nat. Commun. 7, 10465.
Shelkovnikova, T.A., et al., 2013a. Fused in sarcoma (FUS) protein lacking nuclear localization signal (NLS) and major RNA binding motifs triggers proteinopathy and severe motor phenotype in transgenic mice. J. Biol. Chem. 288, 25266–25274.
Shelkovnikova, T.A., et al., 2013b. Recruitment into stress granules prevents irreversible aggregation of FUS protein mislocalized to the cytoplasm. Cell Cycle 12, 3194–3202.
Shelkovnikova, T.A., et al., 2014a. Multistep process of FUS aggregation in the cell cytoplasm involves RNA-dependent and RNA-independent mechanisms. Hum. Mol. Genet. 23, 5211–5226.
Shelkovnikova, T.A., et al., 2014b. Compromised paraspeckle formation as a pathogenic factor in FUSopathies. Hum. Mol. Genet. 23, 2298–2312.
Shelkovnikova, T.A., et al., 2017. Chronically stressed or stress-preconditioned neurons fail to maintain stress granule assembly. Cell Death Dis. 8, e2788.
Shelkovnikova, T.A., et al., 2019. Antiviral immune response as a trigger of FUS Proteinopathy in amyotrophic lateral sclerosis. Cell Rep. 29 (4496–4508), e4.
Sukhanova, M.V., et al., 2020. Fused in sarcoma (FUS) in DNA repair: Tango with poly (ADP-ribose) polymerase 1 and compartmentalisation of damaged DNA. International Journal of Molecular Sciences 21.
Sun, S., et al., 2015. ALS-causative mutations in FUS/TLS confer gain and loss of function by altered association with SMN and U1-snRNP. Nat. Commun. 6, 6171.
Supek, F., et al., 2011. REVIGO summarizes and visualizes long lists of gene ontology terms. PLoS One 6, e21800.
Takanashi, K., Yamaguchi, A., 2014. Aggregation of ALS-linked FUS mutant sequesters RNA binding proteins and impairs RNA granules formation. Biochem. Biophys. Res. Commun. 452, 600–607.
Taylor, J.P., et al., 2016. Decoding ALS: from genes to mechanism. Nature. 539, 197–206.
Turakhiya, A., et al., 2018. ZFAND1 recruits p97 and the 26S proteasome to promote the clearance of Arsenite-induced stress granules. Mol. Cell 70 (906–919), e7.
Vance, C., et al., 2009. Mutations in FUS, an RNA processing protein, cause familial amyotrophic lateral sclerosis type 6. Science. 323, 1208–1211.
Wheeler, J.R., et al., 2017. Isolation of yeast and mammalian stress granule cores. Methods. 126, 12–17.
Yamazaki, T., et al., 2012. FUS-SMN protein interactions link the motor neuron diseases ALS and SMA. Cell Rep. 2, 799–806.
Yasuda, K., et al., 2013. The RNA-binding protein Fus directs translation of localized mRNAs in APC-RNP granules. J. Cell Biol. 203, 737–746.
Youn, J.Y., et al., 2018. High-density proximity mapping reveals the subcellular organization of mRNA-associated granules and bodies. Mol. Cell 69 (517–532), e11.
Zhang, K., et al., 2018. Stress granule assembly disrupts nucleocytoplasmic transport. Cell. 173 (958–971), e17.